New "3D calorimetry" of hot nuclei

E. Vient,[1,*] L. Manduci,[1,2] E. Legouée,[1] L. Augey,[1] E. Bonnet,[3] B. Borderie,[4] R. Bougault,[1] A. Chbihi,[5] D. Dell'Aquila,[4,6] Q. Fable,[5] L. Francalanza,[6] J. D. Frankland,[5] E. Galichet,[4,7] D. Gruyer,[1,8] D. Guinet,[9] M. Henri,[1] M. La Commara,[6] G. Lehaut,[1] N. Le Neindre,[1] I. Lombardo,[6,10] O. Lopez,[1] P. Marini,[11] M. Pârlog,[1,12] M. F. Rivet,[4,†] E. Rosato,[6,†] R. Roy,[13] P. St-Onge,[5,13] G. Spadaccini,[6] G. Verde,[4,10] and M. Vigilante[6]
(INDRA Collaboration)

[1]*Normandie Université, ENSICAEN, UNICAEN, CNRS/IN2P3, LPC Caen, F-14000 Caen, France*
[2]*École des Applications Militaires de l'Énergie Atomique, B.P. 19, F-50115 Cherbourg, France*
[3]*SUBATECH UMR 6457, IMT Atlantique, Université de Nantes, CNRS-IN2P3, 44300 Nantes, France*
[4]*Institut de Physique Nucléaire, CNRS/IN2P3, Université Paris-Sud, Université Paris-Saclay, F-91406 Orsay Cedex, France*
[5]*Grand Accélérateur National d'Ions Lourds (GANIL), CEA/DRF-CNRS/IN2P3, Boulevard Henri Becquerel, 14076 Caen, France*
[6]*Dipartimento di Fisica "E. Pancini" and Sezione INFN, Universitá di Napoli "Federico II," I-80126 Napoli, Italy*
[7]*Conservatoire National des Arts et Métiers, F-75141 Paris Cedex 03, France*
[8]*Sezione INFN di Firenze, Via G. Sansone 1, I-50019 Sesto Fiorentino, Italy*
[9]*IPNL/IN2P3 et Université de Lyon - Université Claude Bernard Lyon 1, 43 Boulevard du 11 Novembre 1918, F-69622 Villeurbanne Cedex, France*
[10]*INFN - Sezione Catania, Via Santa Sofia 64, 95123 Catania, Italy*
[11]*CEA, DAM, DIF, F-91297 Arpajon, France*
[12]*Hulubei National Institute for R&D in Physics and Nuclear Engineering (IFIN-HH), P.O. Box MG-6, RO-76900 Bucharest-Màgurele, Romania*
[13]*Laboratoire de Physique Nucléaire, Université Laval, Québec G1K 7P4, Canada*

(Received 22 September 2017; revised manuscript received 14 September 2018; published 16 October 2018)

In the Fermi energy domain, it is extremely complex to experimentally isolate fragments and particles emitted by a hot nucleus produced during a heavy ion collision. This article presents a new method to characterize more precisely hot quasiprojectiles. It tries to take into account as accurately as possible the distortions generated by all the other potential participants of the nuclear reaction. It is quantitatively shown that this method is an improvement compared to a "classical calorimetry" used with a 4π detector array.

DOI: 10.1103/PhysRevC.98.044611

I. INTRODUCTION

The only way to study experimental nuclear thermodynamics is to produce hot nuclei in nuclear collisions. The hot nuclei are thus obtained in extremely violent and complex conditions. In the Fermi energy domain, we clearly observe a competition between nuclear mean field and nucleon-nucleon interaction during the dissipation of the incident energy of the collision [1,2]. The collisions present mostly an important binary character preserving a very strong memory of the entrance channel [3]. The deeply inelastic diffusion process becomes the dominant phenomenon [4–8]. It is accompanied by an important, thermally unbalanced emission of light particles [8–10]. But we also observe an important production of intermediate mass fragments (IMFs) at the interface of the two colliding nuclei. This latter is usually called *neck emission* [8,11–15]. Fusion is also observed but its cross section becomes small for symmetric collisions above 30 MeV/nucleon [3,16–19]. Obviously, the respective cross sections of these various processes change according to the system, the incident energy, and the impact parameter. The formed hot nuclei deexcite into many particles and fragments. Only a 4π detector array can study such physical processes, because of its detection capabilities. We know that it is fundamental in thermodynamics or statistical mechanics that the system studied be perfectly defined and characterized. This is the main experimental challenge facing nuclear physicists working in the Fermi energy domain. For this reason, the main purpose of this paper is to present, understand, and validate a new method of characterization of an excited quasiprojectile (QP) with a 4π experimental setup in this energy range. By characterization we mean determining its charge, mass, velocity, and excitation energy. We mainly want to improve, possibly, these "measurements" compared to an existing method [20]. This study is presented for the system Xe + Sn at 50 MeV/nucleon detected with the 4π array INDRA [21]. In the first section, we will discuss how to select the products of the quasiprojectile decay from all the particles produced during the reaction. In the following section, we will present the principles of our calorimetry. In the last section, we will study this new experimental calorimetry by comparing it with a "classical calorimetry."

*vient@lpccaen.in2p3.fr; http://caeinfo.in2p3.fr/
†Deceased.

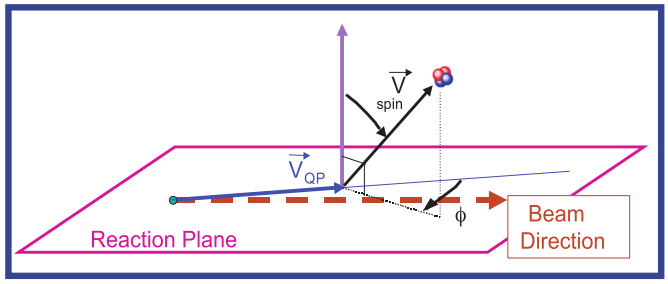

FIG. 1. Definitions of the polar angle θ_{spin} and the azimuthal angle ϕ of a light particle in the QP frame and reaction plane (the azimuthal angle ϕ presented in the figure is negative).

II. IMPROVED SELECTION OF THE EVAPORATED PARTICLES

A. Light particle characterization: Influences of the QP reference frame and of the experimental setup

Here we discuss first how the QP reference frame used in the analysis and the experimental setup may influence the spatial and energetic characteristics of the light charged particles (LCPs) and consequently the determination of the excitation energy of the hot nuclei and the energy spectrum slopes of these particles. For this study, the SIMON event generator, developed by Durand [22], was used. It is set to supply only pure binary collisions Xe + Sn at 50 MeV/nucleon without preequilibrium particles. Evaporation is treated by the Weisskopf theory for light particles and the Kramers transient state theory for fragments. There is a possible secondary emission and a complete calculation in time of the space-time effects of Coulomb interactions between charged particles or fragments produced. We will study different angular distributions of emitted particles. Figure 1 shows the frame used to study the LCP angular distributions and which allows us to define the different used angles. The polar angle θ_{spin} is defined as the angle between the vector normal to the reaction plane and the velocity of a particle in the QP frame. The azimuthal angle ϕ is defined as the angle between the QP velocity in the frame of the center of mass (c.m.) and the normal projection of the velocity of a particle defined in the QP frame on the reaction plane. The azimuthal angle is defined to be positive when the projection of the velocity of the particle on the reaction plane is located to the "left" with respect to the direction of the QP velocity. A particle emitted in the reaction plane and in the direction of the QP velocity will have $\phi = 0^\circ$ and $\theta_{spin} = 90^\circ$. Figure 2 shows two graphs built in the real initial frame of the emitting source, i.e., the QP (which we will call the "true frame"). The generated events were not passed through software simulating the functioning of an experimental apparatus, called the "experimental filter." Therefore, we assume the use of a perfect detector. In this figure, the particles were solely evaporated by the QP according to SIMON. It is important to note that, for all studies with SIMON and comparisons with actual data, only particles located at the front of the center of mass are considered (up to Fig. 7), whatever their origin. The graphs of Fig. 2(a) show the slopes obtained by a Maxwellian fit of α energy spectra, for various angular domains of ϕ and

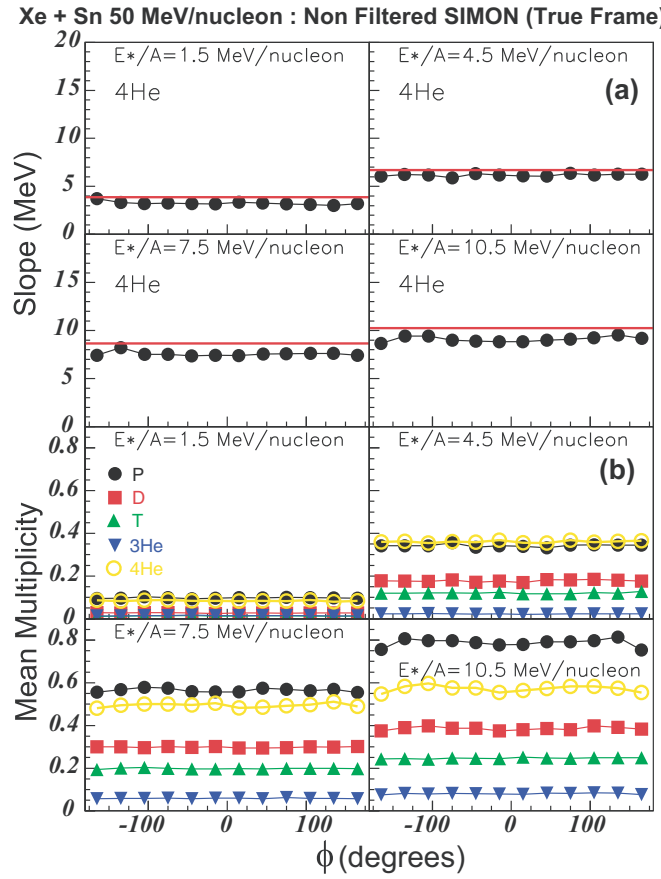

FIG. 2. (a) Slopes of energy spectra of α's evaporated by the QP, obtained by fit for various domains of ϕ, according to the associated mean ϕ. This is done for various selections according to E^*/A of the QP. The red line corresponds to the true initial temperature of the QP, associated with different ranges of excitation energy per nucleon (1 MeV width). (b) Mean multiplicities of the light particles emitted by the QP, generated by SIMON, according to ϕ, without experimental filter, i.e., perfect detection (the velocity being calculated in the true initial frame of the QP). The gray band corresponds to the azimuthal angular range chosen to characterize the QP evaporation.

four different bins of the QP excitation energy per nucleon. The collisions are increasingly violent by from left to right and downward in the figure. The graph in Fig. 2(b) shows the mean multiplicity of light charged particles by azimuthal angle ϕ for the same ranges of excitation energy per nucleon. In both cases, we find the expected result for the emission by a thermalized nucleus, i.e., flat angular distributions for all the light particles and a uniform measured slope regardless of ϕ. This ensures the validity and the consistence of SIMON with respect to the treatment of the isotropic QP decay.

To see and understand the impact of the experimental apparatus, INDRA, we coupled to the generated events by SIMON a program which integrates and simulates all the phases of the ion detection by INDRA (detection efficiency, kinetic energy resolution, angular resolution, isotopic identification). This fundamental stage is referred to as the "INDRA experimental filter." Correct calorimetry requires complete detection of the nuclear reaction products. To try to achieve this goal, we

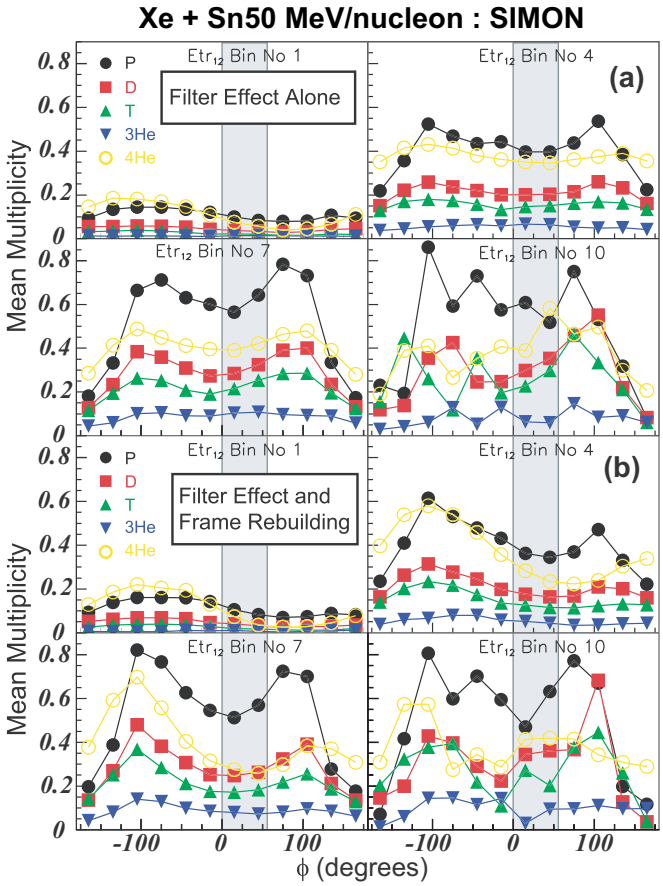

FIG. 3. (a) ϕ distributions of the light particles, located in the forward hemisphere of the center of mass, mainly emitted by the QP, supplied by SIMON after the INDRA filter for various selections according to E_{tr12} (the velocity of each particle being calculated in the true initial frame of the QP). (b) ϕ distributions of the light particles located in the forward hemisphere of the center of mass, mainly emitted by the QP, generated by SIMON, after passage through the INDRA filter, for various selections according to E_{tr12} (the velocity of the particle being calculated here in the rebuilding frame). The considered events are called "complete events." The gray band corresponds to the azimuthal angular range chosen to characterize the QP evaporation.

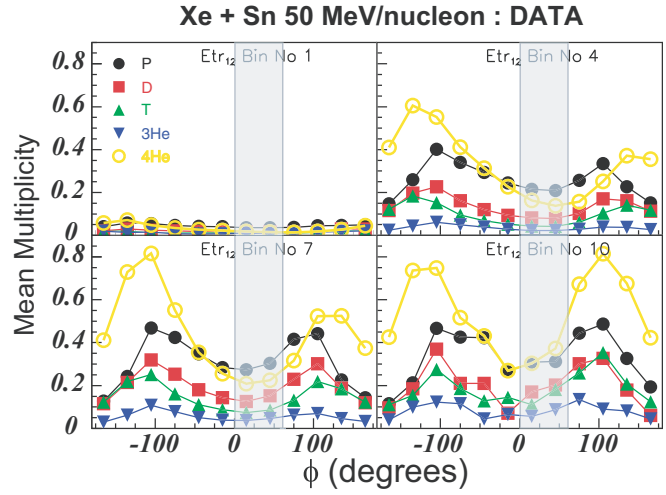

FIG. 4. Experimental azimuthal distributions of the light charged particles located in the forward hemisphere of the center of mass (their velocity being calculated in the reconstructed frame) for various E_{tr12} bins, obtained experimentally with INDRA. The considered events are "complete events." The gray band corresponds to the azimuthal angular range chosen to characterize the QP evaporation.

needed a constraint on the total detected charge and momentum (80% of the initial value) as was done in [23,24]. We also seek to understand the influence of this event selection on calorimetry. These events are hereinafter called "complete events." Indeed, because we do not have an experimental direct access to the excitation energy of the nucleus, we have chosen the total transverse kinetic energy of light charged particles E_{tr12} ($z = 1$ and $z = 2$) as the experimental selector of the violence of the collision [10,25]. In Fig. 3(a), for the complete events, we can observe precisely the sole influence of the INDRA experimental filter on the spatial distribution of particles mainly evaporated by the QP (the frame used here is the true frame of the QP). This selection of complete events implies an important apparent deformation of the ϕ distribution of evaporated particles, even if the velocity of the evaporated particles is defined in the true initial frame. There are apparently more light particles emitted to the right than to the left with respect to the QP velocity, for the peripheral collisions. Indeed, mainly for peripheral collisions, the completeness criterion considers only the events for which the emission of the light particles allowed the QP residue to avoid the hole at the front of the detector, made to let the beam pass. This effect is all the stronger as the QP is focused forwards.

Now, as shown in Fig. 3(b), if the velocity is defined in the reconstructed frame (constructed taking into account intermediate mass fragments and heavy fragments located in the forward hemisphere of the c.m.), we can see that the effect is even more amplified. What is observed in Fig. 3 is the "right-left effect" described in [23,24]. For SIMON, this completeness criterion favors the conservation of isotropic events with a specific topology in the velocity space that allows their detection by INDRA. This significant deformation implies an apparent break of the revolution symmetry of the evaporation around the axis passing through the center of the QP and perpendicular to the reaction plan in the velocity space.

It is questionable whether this apparent effect is merely an artifact related to SIMON. Therefore, we present in Fig. 4 the mean multiplicities of the light charged particles, located at the front of the center of mass, according to ϕ, obtained with the experimental data recorded by the INDRA array. The same trend can be observed, even reinforced because of preequilibrium emission (not taken into account in SIMON) which is preferably between the two partners of the collision, as we can see in the figure. The $\theta_{\rm spin}$ distributions are also modified by the selection criteria and the INDRA experimental filter. In Fig. 5, we present a comparison of the multiplicity distributions of particles at the front of the center of mass as a function of $\cos(\theta_{\rm spin})$ obtained with data [Fig. 5(a)] and pure binary SIMON simulations [Fig. 5(b)] for complete events. We selected semiperipheral collisions by using the LCP total

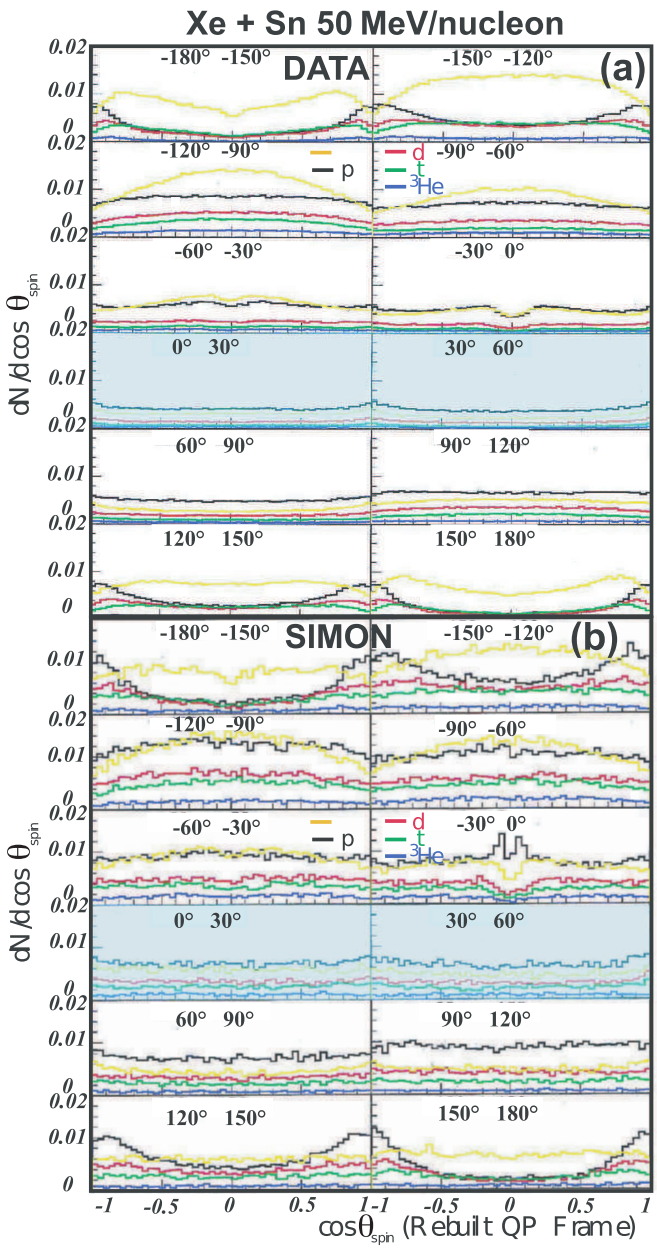

FIG. 5. (a) Multiplicity distributions of the LCPs, located at the front of the center of mass, according to $\cos(\theta_{\rm spin})$ for various ϕ bins. They are obtained for data selection according to the transverse energy corresponding to semiperipheral collisions and also for complete events. (b) The same distributions for data provided by SIMON with the same event selection (the source frame is reconstructed by the experimental method). The blue bands correspond to the azimuthal angular range chosen to characterize the QP evaporation.

transverse kinetic energy. In both cases, we find similar results: there is no apparent symmetry in ϕ. Only the angular domains 0°–30° and 30°–60° are similar. In fact, these trends have been observed already in a study by Steckmeyer *et al.* [23], where the authors showed how the "right-left effect" and the experimental reconstruction method (only from the intermediate mass fragments and heavy fragments at the front of the c.m.) deform the symmetric distribution expected for LCP emissions by a hot rotating source. The required completeness favors events with a pronounced "right-left effect" for peripheral collisions. It was also demonstrated in this study [23] that the space zone, located at the right front in the frame of the reconstructed QP, is strongly polluted by a preequilibrium emission (for semiperipheral and central collisions). There is also a slight pollution of the front of the center of mass by the quasitarget emission, whose importance changes according to the violence of the collision and the type of particle studied, as already noted in Ref. [24]. This contribution, when it exists, is mainly at the back of the QP for central collisions and explains a certain observed forward-backward asymmetry.

Now, for complete events, we will make an equivalent study concerning the energy characteristics of the LCPs in the emitter nucleus frame. First we study the filter effect [in Fig. 6(b)], then the cumulative effect of the filter and the QP velocity reconstruction [in Fig. 6(a)]. The filter and the associated completeness criteria imply apparent modulation of mean kinetic energy according to ϕ, mainly for peripheral collisions. In Fig. 6(a), the addition of the reconstruction effect implies a right-left skewness of the modulation, always linked to the "right-left effect." This phenomenon is more important for α particles. But it is also observed for the other light particles (p, d, t, ^{3}He). It still exists when the physical quantity studied is not the mean kinetic energy but the temperature determined by Maxwellian adjustments of the kinetic energy spectra. Figure 7 shows the experimental data to be compared with the simulation results in Fig. 6(a). There is a significant difference due to the pre-equilibrium emission around $-100°$ and $100°$. Only the zone 0°–60° in ϕ, symbolized by a gray transparent band, seems partially consistent with the expected mean kinetic energy due to evaporation, as shown by the horizontal red line, obtained by considering that the average particle energy should be about twice the temperature measured by adjustment. This trend is also found for the other light particles that are not represented for simplicity. These observations are confirmed by Fig. 8, which shows the experimental energy spectra of tritons, defined in the reconstructed QP frame for various ϕ bins and a transverse energy selection corresponding to semiperipheral collisions. The temperature obtained by fit and the mean energy are indicated. We see again that the particles emitted only in an azimuthal domain between 0° and 60° give spectra compatible with a pure thermal emission by the QP. The spectrum standard deviation, spectrum average energy, and associated temperature indicate that there is an additional contribution in the spectrum corresponding to the azimuthal domain between $-60°$ and 0° in comparison with the spectrum of the azimuthal domain between 0° and 60°. This is also seen for the other light particles. Other studies have been done with the event generator HIPSE [26], which treats more carefully the LCP productions at midrapidity than SIMON. They also show that only a very limited angular domain at the front of the QP is almost not polluted [27]. To illustrate and confirm this, we present in Fig. 9 a comparison of the proton energy distributions obtained with HIPSE (pink graph) and the data (black graph) for complete events and for the different azimuthal angular domains. The collisions studied are semiperipheral. The reaction mechanism selected corresponds to statistical collisions with a medium asymmetry

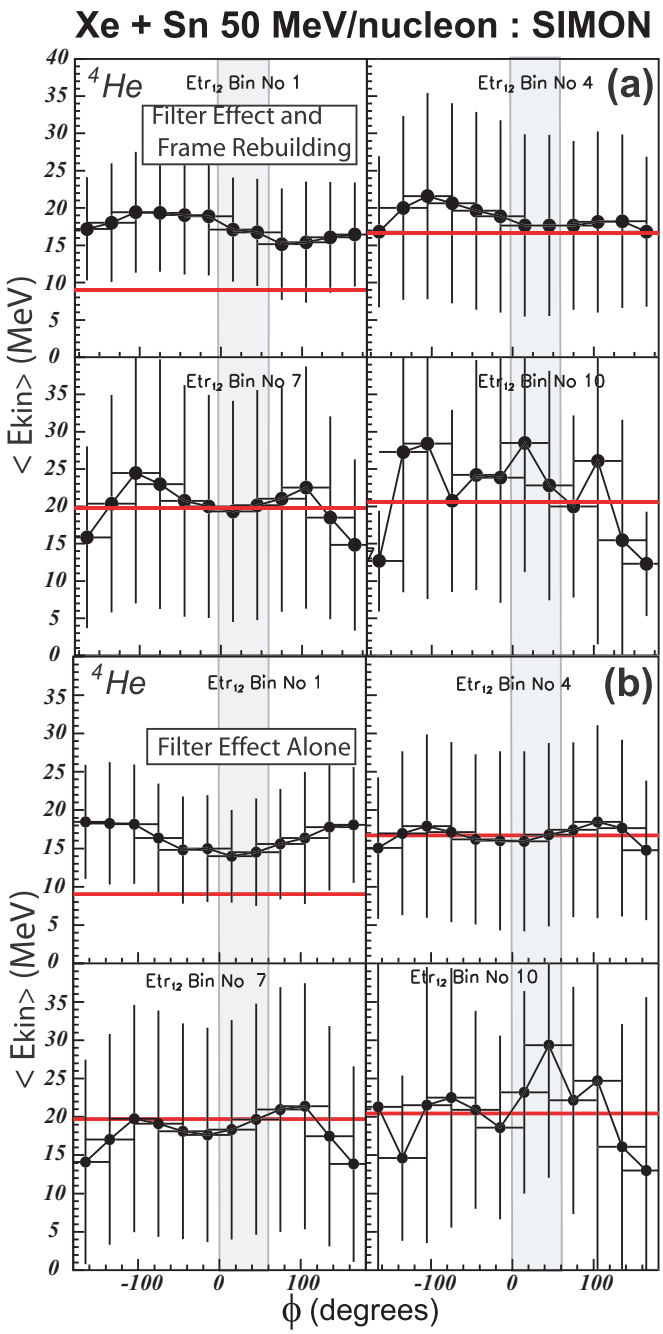

FIG. 6. (a) Mean energy distributions of the α's located in the forward hemisphere of the center of mass according to ϕ, mainly emitted by the QP, generated by SIMON after the INDRA filter (their velocity being calculated in the reconstructed frame) for various E_{tr12} bins. (b) Mean energy distributions of the α's located in the forward hemisphere of the center of mass according to ϕ, mainly emitted by the QP, generated by SIMON after the INDRA filter (their velocities being calculated in the true initial frame) for various E_{tr12} bins. For (a) and (b), the considered events are known as "complete." The red line corresponds to a value twice the expected temperature of the hot nucleus (with a density parameter equal to 10). The gray band corresponds to the azimuthal angular range chosen to characterize the QP evaporation.

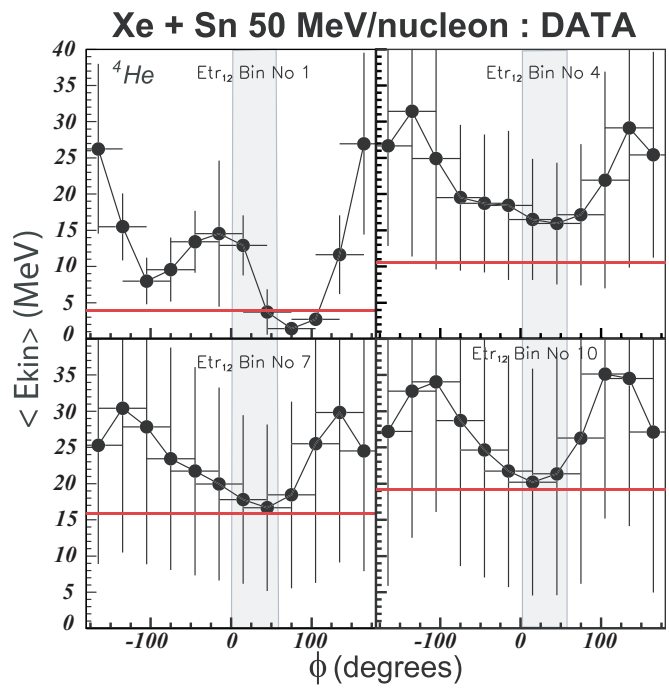

FIG. 7. Mean energy distributions of the α's located in the forward hemisphere of the center of mass according to ϕ and the various selections according to E_{tr12} for the experimental data obtained with INDRA in the reconstructed QP frame. The considered events are events known as "complete." The red line corresponds to two times the measured temperature. The gray band corresponds to the azimuthal angular range chosen to characterize the QP evaporation.

(see Sec. II B). Histograms of HIPSE and data are normalized to match the same number of events (in the E_{tr12} norm bin). The agreement between HIPSE and the data is quite remarkable for protons for all angular domains. HIPSE offers the opportunity of knowing the true origin of the nuclei produced during a collision. We were able to construct the spectra of the protons actually evaporated by the QP (blue graph) and the spectra of the protons having another origin (green graph) for all the azimuthal angular domains. We see clearly that the least disturbed azimuthal angular range is 0°–60° even if there is proton pollution from other sources in this range according to HIPSE. This type of result had also been pointed out using Landau-Vlasov calculations but for smaller systems, in Ref. [28]. The mean value and the standard deviation of the kinetic energy distribution of the data are the lowest for this azimuthal angular range. The average proton multiplicity is also the smallest for this one. All these facts indicate that this is the zone of velocity space in the reconstructed QP frame least polluted by contributions that were not evaporated by the QP. This is also observed for the other types of light particles for data and for HIPSE, for the other reaction mechanisms [27].

B. The importance of selecting the reaction mechanism

As already discussed in the Introduction, different reaction mechanisms can be observed in intermediate energy heavy ion reactions. We defined selection criteria to separate purely binary collisions followed by a standard statistical decay and

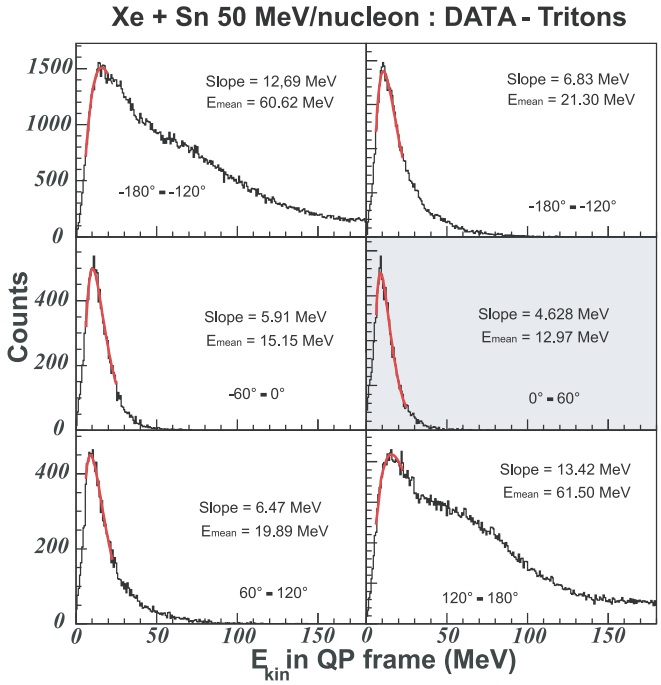

FIG. 8. Kinetic energy distributions of the tritons in the reconstructed frame of the QP, for various angular selections according to ϕ obtained by the INDRA Collaboration for the system Xe + Sn at 50 MeV/nucleon. The events are complete and correspond to semiperipheral collisions. The red lines correspond to the best fit of each spectrum (the obtained temperatures from slope and mean energy are indicated). The gray band corresponds to the azimuthal angular range chosen to characterize the QP evaporation.

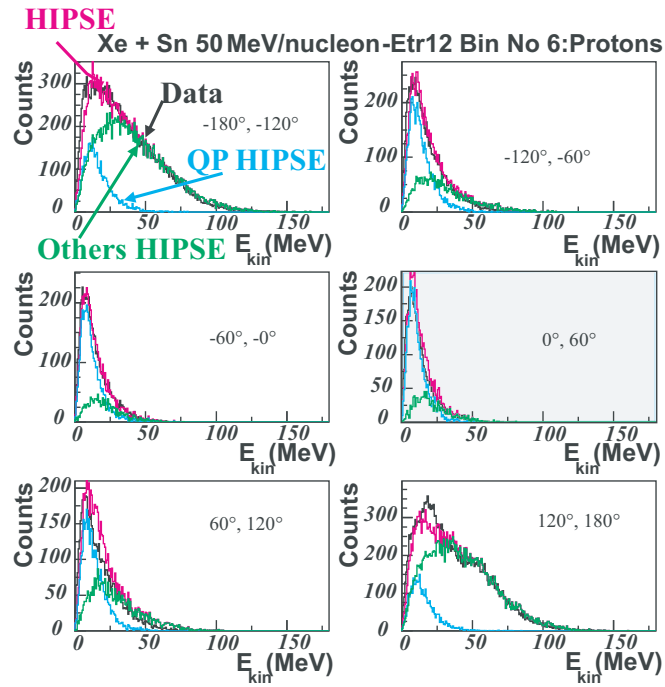

FIG. 9. Kinetic energy distributions of the protons in the reconstructed frame of the QP, for various angular selections according to ϕ obtained for the system Xe + Sn at 50 MeV/nucleon. The events are complete and correspond to semiperipheral collisions. The data correspond to the black curves, HIPSE to pink. The protons emitted by the QP according to HIPSE are associated with the blue curves, the others with the green ones. The gray band corresponds to the azimuthal angular range chosen to characterize the QP evaporation.

collisions with the formation of a matter neck. We will call the former *statistical* collision and the latter *neck emission*. It was shown in [27,29,30] that a valid criterion to identify an event as a statistical collision is the presence of the second heaviest fragment at the front of the center of mass, in the forward hemisphere of the QP frame (see Fig. 10). Neck emission events are those with midrapidity emission (nuclear matter between the two partners of the binary collision). This discrimination makes it possible to isolate binary collisions followed by statistical emission. The latter seems to be a more appropriate scenario for the theoretical bases of our reconstruction method of the hot nucleus. It has already been shown and discussed in Refs. [27,29,30] that these two mechanisms correspond to very different dynamics. The energy dissipation process can have different origins, as reported in Ref. [29]. We want to see if we are actually able to observe differences between these mechanisms thanks to three-dimensional (3D) calorimetry. In Fig. 11, to select the violence of the collision we have chosen to use the variable E_{tr12} normalized to the available energy in the center of mass in the direction perpendicular to the beam. This variable provides a good indication of dissipation during a reaction [3,31]. A total dissipation of incident energy (in the sense of complete thermalization) should give a value of 1 for this variable.

We also use the variable η which characterizes the charge asymmetry between the two heaviest fragments at the front of the center of mass:

$$\eta = (Z_{\max 1} - Z_{\max 2})/(Z_{\max 1} + Z_{\max 2}). \quad (1)$$

This variable was used to obtain a bimodality signal to characterize a possible liquid-gas phase transition in hot nuclei

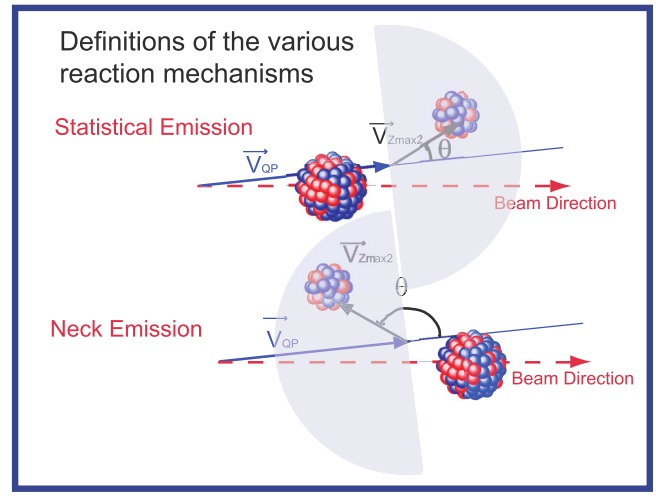

FIG. 10. Diagram plotting the selection criteria of the two studied reaction mechanisms.

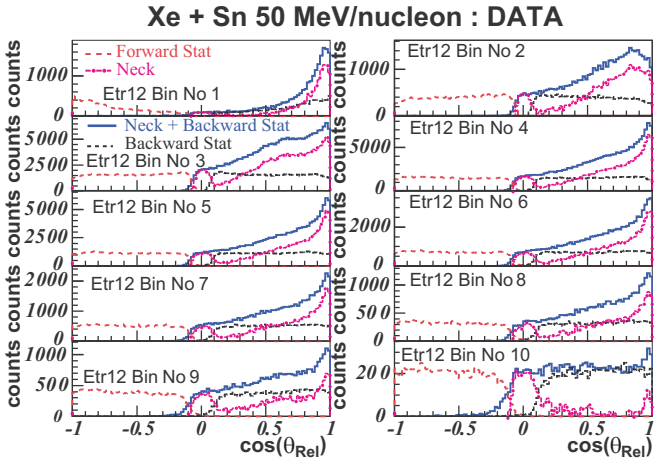

FIG. 11. Distributions of the cosine of the angle $\theta_{\rm rel}$, presented for events having a medium charge asymmetry between the two largest fragments of the event and for various selections: the blue full line corresponds to the neck emission, the red dashed line on the left corresponds to the statistical emission at the front of the QP frame, the black dashed line on the right corresponds to the backward QP emission, and the pink dash-dotted line corresponds to the pure neck emission for which the statistical contribution has been subtracted. The violence of the collision increases as you go from left to right and downward.

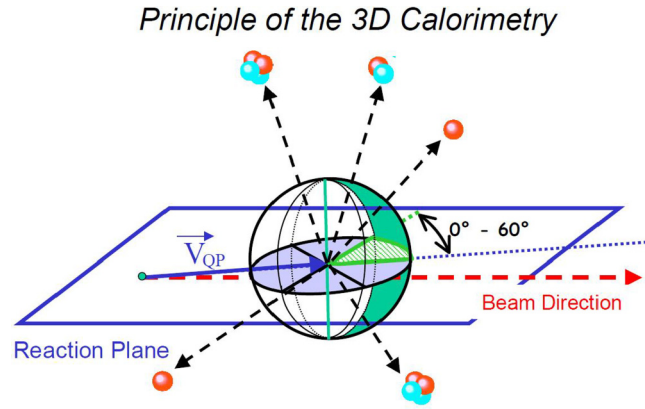

FIG. 12. Diagram allowing visualization the considered spatial domain to define the probability of exmission by the QP for all types of particles.

[32–34]. This signal corresponds to the passage from the deexcitation of the hot nucleus by a standard evaporation to that by multifragmentation. So it seems interesting to see what the 3D calorimetry gives in this context, hence this additional selection variable.

Figure 11 shows, for various collision violence ranges (different zones of normalized E_{tr12}), the distribution of the cosine of $\theta_{\rm rel}$, the angle between the relative velocity $\overrightarrow{V_{\rm rel}}$ of the two heaviest fragments at the front of the center of mass [see the definition in Eq. (2)] and the velocity of the reconstructed source $\overrightarrow{V}_{\rm QP}$. This relative velocity is defined by the following relationship:

$$\overrightarrow{V_{\rm rel}} = \overrightarrow{V}_{Z_{\rm max1}} - \overrightarrow{V}_{Z_{\rm max2}}. \qquad (2)$$

We limit ourselves here to present typical cases: collisions for the system Xe + Sn at 50 MeV/nucleon, having a medium asymmetry between the two heaviest fragments (i.e., $0.33 < \eta \leqslant 0.66$).

It can be noted that events labeled as statistical (red dashed line) have a flat distribution, if one neglects some angular acceptance problems, which are more visible for the peripheral collisions. For these events, if the second largest fragment is at the front of the QP, then the largest is at the back; therefore the relative vector between the two is oriented opposite to the reconstructed QP vector. The events with a neck (blue full lines) present a focus of the relative velocity in the direction of the velocity of the reconstructed source. This focusing effect is greater when the collision is less violent. To improve the selection of this contribution, one can subtract the statistical backward distribution, for which the second heaviest fragment would be emitted backward with respect to the QP. This back statistical distribution should be the symmetrical distribution of events known as statistical, as we select them, relative to the zero abscissa of the distribution (black dashed line). It shall give positive relative angle values, taking into account the definition of the relative velocity. After subtraction, a clean $\cos\theta_{\rm rel}$ distribution of the events corresponding to the genuine neck emission, i.e., *pure neck emission* (pink dash-dotted line in Fig. 11) is obtained. The distribution shape does not change, but the proportion of events can be estimated more carefully. This contribution tends to disappear as the violence of the collision increases. In fact, we choose to keep both mechanisms to see if differences appear when we apply our new calorimetry.

III. THE NEW "3D CALORIMETRY"

A. Determination of the clean spatial domain of the QP emission

Studies reported in Refs. [23,24] and the conclusions drawn in Sec. II A convinced us that, to correctly characterize QP deexcitation, we must use a fairly narrow spatial domain. Based on the angular definitions of ϕ and of $\theta_{\rm spin}$ given in Sec. II A, we consider following particles actually emitted only by the QP: the particles located in the azimuthal angular domain included between 0° and 60° in the reconstructed QP frame. This corresponds to one sixth of the total solid angle, as shown in Fig. 12. This spatial domain is, by definition, linked to the QP velocity reconstructed in the center-of-mass frame. It changes from one event to another and will change according to the different selections on the violence of the collision. The quasiprojectile is then reconstructed, event by event, by assigning to each particle a given emission probability, which has been determined using all the information obtained in the space xdomain defined above. This type of calorimetry was partially used in a simplistic way in [35].

B. Calculation of the emission probabilities by the QP

To apply this 3D calorimetry and define the emission probability by the QP, we assume that the QP deexcitation process presents a symmetry of revolution around the axis

perpendicular to the reaction plane described by the reconstructed velocity of the QP and the velocity of the initial projectile. The angular momentum of the QP must be, on average, in this direction perpendicular to the reaction plane due to conservation laws. The latter must therefore not break the symmetry of revolution around this same axis for the evaporation of particles by the QP. We defined, for ϕ ranging from -180° to 180°, six areas 60° wide. Initially, for each of them, we constructed all the polar angular distributions as well as the energy distributions for all the types of detected particles, defined in the frame of the reconstructed QP. This is done by using all the light particles and the intermediate mass fragments, except for the two heaviest fragments emitted at the front of the center of mass (the probability is 1 that both nuclei come from the QP). From these distributions, for an angular domain between ϕ_1 and ϕ_2, we determine an experimental emission probability by the QP for a particle of kinetic energy E_k at an angle θ_{spin} and in an azimuthal angular domain $\Delta\phi$: $\text{Prob}(E_k, \theta_{\text{spin}}, \Delta\phi = \phi_1 - \phi_2)$.

We first assume that for any particle the probability of being emitted in a polar angle θ_{spin} is independent of kinetic energy and vice versa. This means that we neglect the influence of the angular momentum on the distribution of kinetic energy. Based on this assumption, the probability can therefore be calculated from the following relation:

$$\text{Prob}(E_k, \theta_{\text{spin}}, \Delta\phi) = \text{Prob}(E_k, \Delta\phi) \times \text{Prob}(\theta_{\text{spin}}, \Delta\phi). \tag{3}$$

From this last relation and our choice of selection of particles emitted by the QP, we deduce that the experimental probability is given by the following relation:

$$\text{Prob}(E_k, \theta_{\text{spin}}, \phi_1 - \phi_2) = \frac{\frac{dN(E_k, 0^\circ - 60^\circ)}{dE_k}}{\frac{dN(E_k, \phi_1 - \phi_2)}{dE_k}} \times \frac{\frac{dN(\theta_{\text{spin}}, 0^\circ - 60^\circ)}{d\cos\theta_{\text{spin}}}}{\frac{dN(\theta, \phi_1 - \phi_2)}{d\cos\theta_{\text{spin}}}}. \tag{4}$$

An example of the experimental determination of the probability distribution of emission of a proton by the QP as a function of its kinetic energy in the reconstructed frame is shown in Fig. 13. We have in mind that, in the angular domains other than the reference one, there are necessarily particles in addition to the particles evaporated by the QP since they are polluted by other contributions. This is what we see with the actual data and what is confirmed when we study the energy or angular distributions provided by HIPSE, such as the one presented in Fig. 9. This calculation is also done for event selections according to the violence of the collision, the reaction mechanism, and the asymmetry between the two heaviest fragments at the front. Furthermore, the chosen completeness criteria are here less drastic than previously, and they focus on the reconstruction of the QP. The events studied here are complete events at the front of the center of mass. For these events, we can observe in Fig. 14 the proportion of the different selections of mechanism and decay taken into account in this study according to the violence of the collision. We observe a statistical contribution to the front which is relatively constant around 30–35% (we remember that this number must be doubled to obtain the right proportion of events corresponding to the statistical emission).

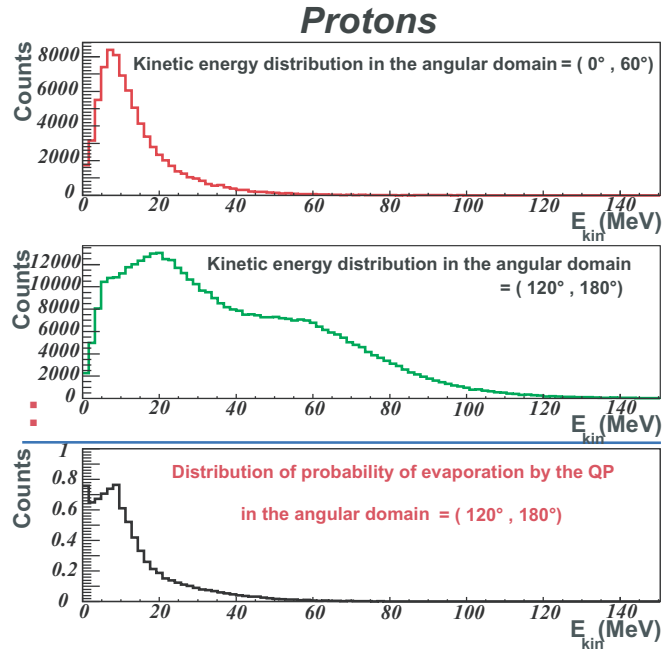

FIG. 13. Principle for calculating the experimental distribution of probability $\text{Prob}(E_k, \Delta\phi)$ for a proton to be evaporated by the QP as a function of its kinetic energy in the QP frame for a given azimuthal angular domain.

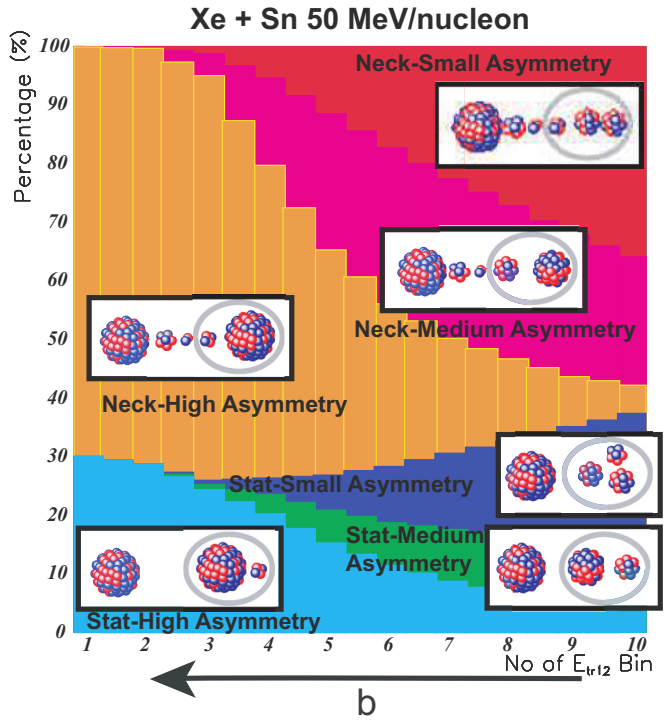

FIG. 14. Proportions of the various types of reaction mechanisms according to the violence of the collision for the system Xe + Sn at 50 MeV/nucleon.

We thus obtain experimental probability functions depending on the following variables:

$$\mathrm{Prob}(E_k, \theta_{\mathrm{spin}}, \phi_1 - \phi_2, E_{tr12}\,\mathrm{norm}, \eta, \mathrm{mechanism}, Z, A)$$

for the particles of charge $Z \leqslant 3$, identified also by mass;

$$\mathrm{Prob}(E_k, \theta_{\mathrm{spin}}, \phi_1 - \phi_2, E_{tr12}\ \mathrm{norm}, \eta, \mathrm{mechanism}, Z)$$

for the particles of charge $Z > 3$.

We note that we have assumed here that the probability of detection is independent of E_k, θ_{spin}, and ϕ.

C. QP reconstruction

For each particle $(Z_n, A_n, \overrightarrow{P_n})$ detected in an event, we determine its kinetic energy E_k and the polar angle θ_{spin} and azimuthal angle ϕ of its velocity, defined in the reconstructed frame. We thus deduce its probability Prob_n of being emitted by the QP from the experimental functions of probability [see Eq. (4)]. This probability is then associated with this particle to reconstruct the characteristics of the QP. The QP charge can be estimated as follows:

$$Z_{\mathrm{QP}} = \sum_{n=1}^{\mathrm{multot}} \mathrm{Prob}_n \times Z_n, \tag{5}$$

where multot is the number of detected charged particles in the event. For the mass, we have to make assumptions. We assume that the QP keeps the isotopic ratio of the initial projectile and that the nuclei follow the valley of stability. Mass conservation allows us to deduce the number of neutrons produced by the QP, as indicated by the relation

$$A_{\mathrm{QP}} = Z_{\mathrm{QP}} \times 129/54 = \sum_{n=1}^{\mathrm{multot}} \mathrm{Prob}_n \times A_n + N_{\mathrm{neutron}}. \tag{6}$$

We can then deduce the reaction Q value,

$$Q = E_b(A_{\mathrm{QP}}, Z_{\mathrm{QP}}) - \sum_{n=1}^{\mathrm{multot}} \mathrm{Prob}_n \times E_b(A_n, Z_n) - N_{\mathrm{neutron}} \times E_b(1, 0). \tag{7}$$

$E_b(A_n, Z_n)$ is the binding energy of the nucleus ${}^{A_n}_{Z_n}X$.

We determine the QP velocity in the frame of the center of mass of the reaction only from charged particles by using the following expression:

$$\overrightarrow{V}_{\mathrm{QP}} = \frac{\sum_{n=1}^{\mathrm{multot}} \mathrm{Prob}_n \times \overrightarrow{P_n}}{(A_{\mathrm{QP}} - N_{\mathrm{neutron}})}, \tag{8}$$

with $\overrightarrow{P_n}$ the linear momentum of the nth particle in the frame of the center of mass.

We can then calculate the QP excitation energy:

$$E^*_{\mathrm{QP}} = \sum_{n=1}^{\mathrm{multot}} \mathrm{Prob}_n \times E_{kn} + N_{\mathrm{neutron}} \times \langle E_k \rangle_{p+\alpha} - Q - E_{kQP}, \tag{9}$$

E_{kn} being the kinetic energy of the nth particle in the center-of-mass frame, $\langle E_k \rangle_{p+\alpha}$ the mean kinetic energy of the neutrons deduced from that of the protons and α's (Coulomb energy is subtracted), and finally E_{kQP} the QP kinetic energy in the center-of-mass frame.

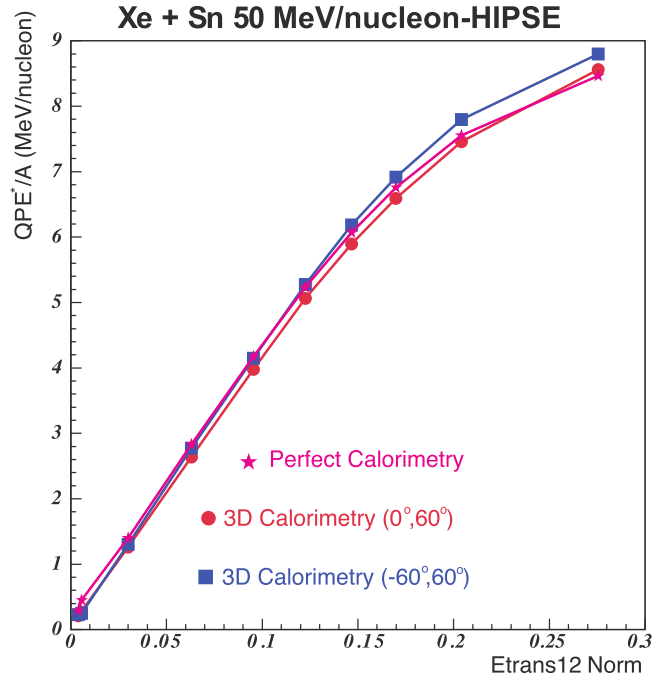

FIG. 15. Average correlations between QP excitation energy per nucleon measured by different calorimetries and the normalized transverse energy of LCPs obtained for filtered and complete HIPSE events for the system Xe + Sn at 50 MeV/nucleon.

To finish this subsection, we would like to remind the reader that this calorimetry has been created essentially because of the study presented in Ref. [23], as indicated at the beginning of this section. This calorimetry shows very clearly in Fig. 9 of this article, for semiperipheral collisions, that even the front of the QP is polluted by contributions not coming from the QP. Only a part of this area in front did not seem to be polluted (positive angles up to 90°). This result implied that calorimetries doubling the forward component of the QP were incorrect. This is the reason of our choice to do a different calorimetry and to take a limited positive angular domain 0°–60°. One may wonder, however, whether this is not too restrictive and drastic. Some preceding figures, such as Figs. 8 and 9 for example, seem to show that the angular domain −60°–0° is very similar to the angular domain chosen as reference, even if on average it appears a little more energetic. To verify this, we performed 3D calorimetry with the data provided by HIPSE for the Xe + Sn system at 50 MeV/nucleon using the angular domain −60°–60° as reference to determine the evaporation probabilities. In HIPSE, the produced nuclei are marked according to their origin, thus making it possible to make a perfect QP calorimetry with the nuclei emitted by the QP and detected by INDRA.

We present in Fig. 15 a comparison between the two 3D calorimetries with different angular reference domains and the perfect calorimetry according to the normalized LCP transverse energy. This is done without any selection of reaction mechanisms. We immediately notice that the

two 3D calorimetries are very close to each other and to the perfect calorimetry up to 6 MeV/nucleon, for the most peripheral collisions. A small difference appears for more central collisions with an excess of excitation energy per nucleon for 3D calorimetry using −60°–60° compared to the other two, perhaps indicating a small pollution of the added area.

IV. COMPARISON WITH A "CLASSICAL CALORIMETRY"

As a rough guide, we will compare this "3D calorimetry" with a "classical calorimetry" based on a technique doubling the particle contribution at the front of the QP, described in [20], as used by the INDRA and MULTICS Collaborations for the QP calorimetry. It is used in Refs. [23,24,32,33,36], for example.

Figure 16 shows the average evolution of the QP charge and excitation energy per nucleon for the different selections of interest. Figure 16(a) shows the excitation energy per nucleon for the two different calorimetries and the dissipated energy per nucleon during the collision. The latter is determined from the measured QP velocity by our calorimetry. As indicated in Ref. [3], we can obtain the amount of the initial incident energy in MeV, which is dissipated per nucleon during the collision by the following expression:

$$\frac{E_{\text{Dissipated}}}{A} = \frac{E_{\text{CM}}}{(A_{\text{Proj}} + A_{\text{Tar}})} - \frac{1}{8} \times \frac{V_{\text{rel}}^2}{c^2} \times 1\ \text{amu}\, c^2, \qquad (10)$$

with E_{CM} the available energy in the center of mass of the reaction and V_{rel} the relative velocity between partners of the collision.

Here, since the system is symmetric, we assume that $V_{\text{rel}} \simeq 2 \times V_{\text{QP}}$, with V_{QP} the QP velocity in the center-of-mass frame. Equation (10) is only valid for symmetric systems and assumes that preequilibrium emission is symmetric in the center-of-mass frame. This energy therefore represents the maximum energy that can be stored by the QP. Figure 16(a) shows, for each type of mechanism and asymmetry, the curves for the excitation energy per nucleon obtained by 3D calorimetry (red circles), "classical calorimetry" (green squares), and the dissipated energy per nucleon (blue triangles). In this figure, it is immediately evident that there is a visible qualitative improvement in the measures. With the new calorimetry, for the most peripheral collisions, we obtain lower limit values that seem reasonable: they are close to $E^*_{\text{QP}} = 0$ MeV/nucleon for excitation energy per nucleon and $Z_{\text{QP}} = 54$ for QP charge [Fig. 16(b)], which is not always the case for "classical calorimetry." Moreover, unlike the classical method, the measured excitation energy never exceeds the estimated dissipated energy. There is, therefore, a reasonable consistency between the measured QP velocity and the measured excitation energy per nucleon.

With regard to the measurement of the QP charge in Fig. 16(b), the very different measurements, obtained with the "classical calorimetry," between events called statistical and events with a neck emission, disappear completely with the new 3D calorimetry. The standard deviations shown are also significantly smaller.

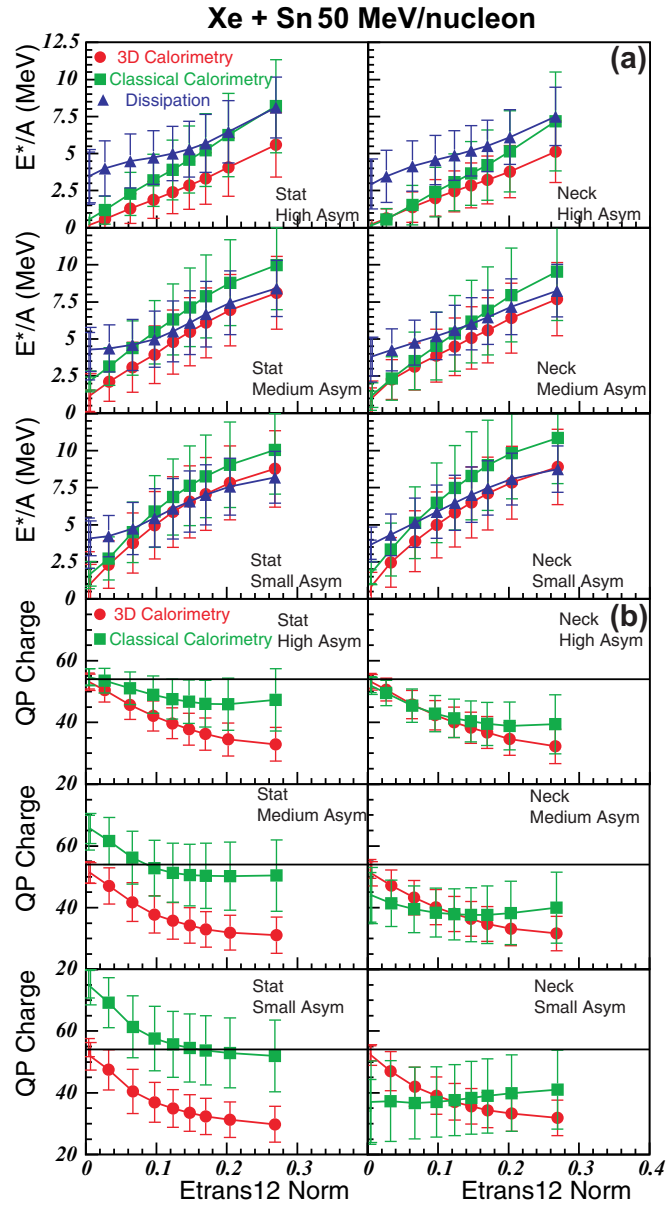

FIG. 16. (a) Average correlation between the measured QP excitation energy per nucleon and the normalized transverse energy of LCPs for various selections of mechanism and asymmetry for collisions Xe + Sn at 50 MeV/nucleon. (b) Average correlation between the QP reconstructed charge and the normalized transverse energy of LCPs for various selections of mechanism and asymmetry for collisions Xe + Sn at 50 MeV/nucleon (the black line indicates the projectile charge).

This simple comparison is not naturally sufficient to validate this new calorimetry, but it shows that this 3D calorimetry improves the measurement of the QP (E^*_{QP} and Z_{QP}). It seems essential to study it by means of a simulation that is as realistic as possible. This is done systematically with HIPSE for the system Xe + Sn at different incident energies in Ref. [37], comparing with actual data.

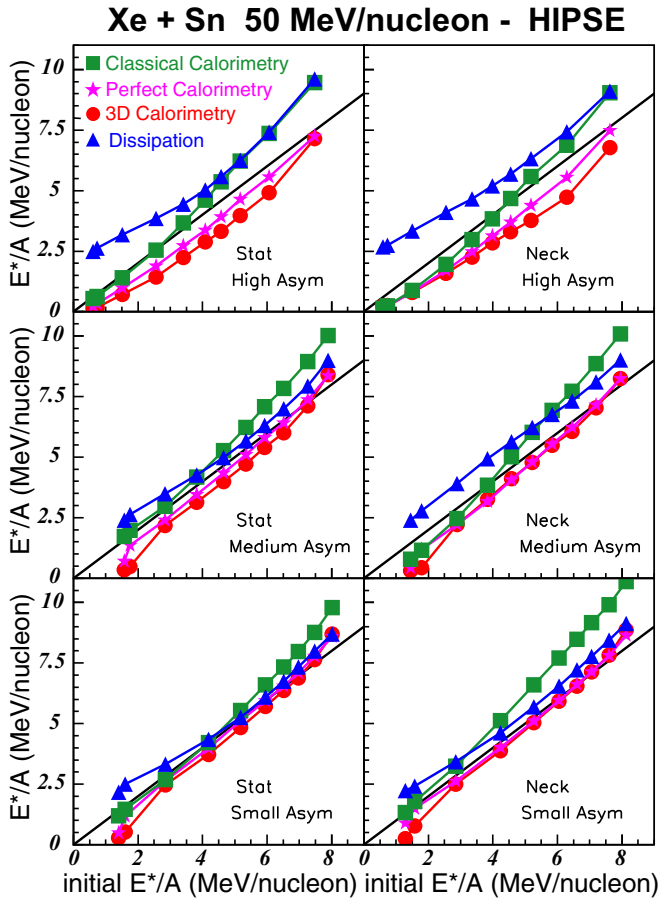

FIG. 17. Average correlations between the initial QP excitation energy per nucleon given by HIPSE and the estimations of this physical quantity by different calorimetric methods for various mechanism selections and asymmetry for collisions Xe + Sn at 50 MeV/nucleon. The green squares correspond to "classical calorimetry," the pink stars to perfect calorimetry done with HIPSE labeling, the red circles to 3D calorimetry, and the blue triangles to energy dissipation from the QP velocity. The events provided by HIPSE have been filtered and selected exactly according to the same criteria as the actual data.

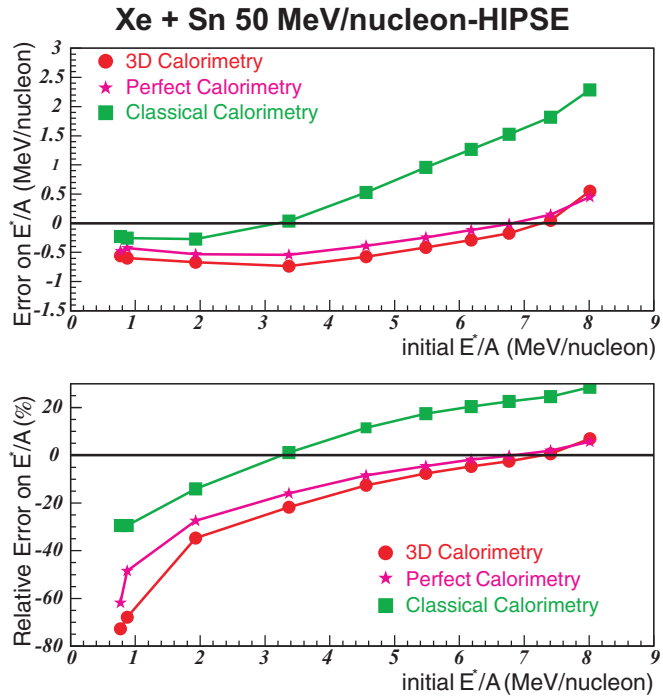

FIG. 18. Average correlations between the initial QP excitation energy per nucleon given by HIPSE and the estimations of the absolute and relative errors on the QP excitation energy per nucleon obtained by different calorimetric methods for collisions Xe + Sn at 50 MeV/nucleon. The green squares correspond to "classical calorimetry," the pink stars to perfect calorimetry done with HIPSE labeling, and the red circles to 3D calorimetry. The events provided by HIPSE have been filtered and selected as complete at the front of the center of mass but without a reaction mechanism selection.

We can fully understand the interest of this study to validate 3D calorimetry through Fig. 17. This allows us to fully confirm the findings shown in Fig. 16. Using the "INDRA experimental filter" and the HIPSE event generator, it is possible to verify whether our calorimetry is capable of experimentally recovering the initial excitation energy of QPs created by simulation. After passing all the events for the Xe + Sn system to 50 MeV/nucleon (3 million) through the experimental filter, it is possible to fully apply all the event selections used for the real data and indicated in this article. With HIPSE, for events detected and kept because they are complete, we know the true initial excitation energy of the quasiprojectile. We can moreover apply 3D calorimetry or "classical calorimetry" for all these events using only the nuclei actually detected by INDRA. We also apply the perfect calorimetry provided by HIPSE, as explained above. We can thus present in Fig. 17 the average evolution of these three different calorimetries as a function of the initial excitation energy of the quasiprojectile for the different reaction mechanisms studied. We added in the figure the energy dissipated by nucleon obtained, as previously explained. The results obtained are very similar to those observed with the actual data in Fig. 16 when we compare 3D calorimetry, "classical calorimetry," and dissipation. Comparison with perfect calorimetry confirms that 3D calorimetry is significantly better than "classical calorimetry." The smaller the asymmetry, the closer the 3D calorimetry is to perfect calorimetry. It is for collisions with neck that the agreement is better. However, it should be noted that these curves are not perfectly aligned with the black lines corresponding to a perfect measurement of the QP excitation energy, even for a perfect calorimetry. There are clearly effects associated with the experimental setup. The completeness criterion generates a specific topology of events in the velocity space, which disrupts the calorimetry. This is mainly visible for events with a large asymmetry. The detection efficiency removes QP particles unevenly as a function of their kinetic energy in the QP frame.

To observe an eventual influence on the quality of excitation energy per nucleon measurement related to reaction mechanism selections, we also present in Fig. 18 the absolute and relative errors on the measurement of excitation energy

per nucleon as a function of the initial excitation energy per nucleon of QP, when these three calorimetries are applied to the HIPSE data filtered by INDRA, without any reaction mechanism selection. We immediately notice the excellent agreement between 3D calorimetry and perfect calorimetry. The classical calorimetry appears very different, except perhaps for the least dissipative and therefore most peripheral collisions. These results are consistent with what is observed in Fig. 17. The results for "classical calorimetry" are very similar to those obtained with a version of SIMON without preequilibrium in Ref. [24]. It is also clear from this figure that it is necessary to correct the detection efficiency in order to be able to more correctly recover the excitation energy per nucleon of the QP. This work remains to be done and is complex. One possibility would be to determine, using HIPSE and the software simulating INDRA functioning, the probability that a particle evaporated by the QP, of kinetic energy given in the QP reference frame, emitted at given polar and azimuthal angles, will actually be detected. It would then just be necessary to correct the probability associated with the particle, taking into account this efficiency. But this is a correction that depends on the model used.

V. CONCLUSIONS

By causing extremely violent heavy ion collisions, nuclear physicists attempt to modify the internal energy of the nucleus. In the Fermi energy domain, the way in which this energy is deposited and stored is still a subject of much discussion. This is mainly due to the fact that it is very difficult to prove unequivocally that a hot nucleus, thermodynamically well equilibrated, has been formed. In this context, we have described the basis for a method of QP reconstruction and reviewed the difficulties which can intervene.

We have chosen an experimental approach to try to gradually resolve the difficulties. To do this, we used the SIMON event generator and a simulation program, reproducing as closely as possible the behavior of our experimental device.

First, in the context of binary collisions generated by SIMON without pre-equilibrium, we have studied the deexcitation of a hot quasiprojectile. We have observed significant spatial and energetic apparent distortions of the particles evaporated by the QP. We have shown the fundamental roles played by the experimental setup and the recoil effects when we impose the completeness of the events. Indeed, for a correct calorimetry, all fragments and particles evaporated by the QP must be detected. Therefore, we must use events called "complete events." For very peripheral collisions, detection of the QP residue remains difficult due to the forward acceptance of INDRA. For collisions where few particles are evaporated, they must have a large linear transverse momentum to properly deflect the QP residue allowing its detection. "Complete events" correspond mainly to these type of events for peripheral collisions. It is difficult to compensate for the recoil effect caused by the emission of the first evaporated particle. Therefore, we do not find isotropic spatial and energetic distributions, but a recoil effect called "right-left," which is dominant for peripheral collisions, even if the QP emission in SIMON is basically isotropic for all events. It also indirectly implies difficulties in determining the source velocity, when only IMFs and heavy fragments are used to reconstruct the hot nucleus frame. There is clearly a difference between the IMFs' and LCPs' centers of mass, which implies an apparent energy contribution of LCPs too large in the reconstructed frame of the QP. All these facts are confirmed with the real experimental data and even amplified by preequilibrium contribution.

Second, we introduced a new calorimetry protocol to better characterize the quasiprojectile. This calorimetry is based on the experimental determination of an emission probability from the physical characteristics of particles in a restricted area of the velocity space. We wanted it to be able to take into account the influence of preequilibrium particles and of a possible contribution of midrapidity such as the neck emission.

In this study, we added additional event selection criteria to observe the robustness of this calorimetry. We have differentiated between collisions with neck emission and others. We also took into account the asymmetry between the two heaviest fragments at the front of the center of mass. It is one of the important parameters for studying the phase transition in nuclear matter.

To fully demonstrate the interest of 3D calorimetry, we compared it to a "classical calorimetry" that consists of doubling of the light charged particles located at the front of the reconstructed frame. The latter seems clearly inaccurate. It tends to give excitation energies per nucleon that are too high in comparison to the apparent dissipation, as can be clearly seen in Figs. 16 and 17. It also provides too wide distributions of excitation energy per nucleon or charge for the reconstructed QP [24]. This calls into question the quality of selections made with an excitation energy obtained with "classical calorimetry" like this. The new calorimetry provides better estimates of the excitation energy per nucleon than previous methods, as shown in Figs. 17 and 18. But, by its intrinsic hypotheses (two sources of particles), it can allow one to make a correct physical characterization of only binary collisions, i.e., peripheral or semiperipheral collisions. A complementary and complete analysis of these qualities and defects is made in Ref. [37] for the system Xe +Sn at different incident energies.

To complete our conclusion on this study, we note that a real improvement in the quantitative characterization of the QP can only be achieved by an effective correction of the complex distortions generated by the experimental device and event selection criteria, or by the construction of a 4π detector, which would have a better granularity, an efficient forward detection, and an excellent isotopic resolution, improving particle identification and kinematic characterization. We must finally bear in mind that all these conclusions can only be drawn in principle for the studied system, Xe + Sn, and are to be confirmed for the others. On the other hand, this work clearly confirms that a comparison between a theoretical model and experimental data makes sense in this domain of physics only if the theoretical model passes through a software filter that simulates the entire detector response.

[1] G. Lehaut, D. Durand, O. Lopez, E. Vient, A. Chbihi, J. D. Frankland, E. Bonnet, B. Borderie, R. Bougault, E. Galichet, D. Guinet, Ph. Lautesse, N. Le Neindre, P. Napolitani, M. Parlog, M. F. Rivet, and E. Rosato, Phys. Rev. Lett. **104**, 232701 (2010).

[2] O. Lopez, D. Durand, G. Lehaut, B. Borderie, J. D. Frankland, M. F. Rivet, R. Bougault, A. Chbihi, E. Galichet, D. Guinet, M. La Commara, N. Le Neindre, I. Lombardo, L. Manduci, P. Marini, P. Napolitani, M. Pârlog, E. Rosato, G. Spadaccini, E. Vient, and M. Vigilante, Phys. Rev. C **90**, 064602 (2014).

[3] V. Métivier *et al.*, Nucl. Phys. A **672**, 357 (2000).

[4] J. C. Steckmeyer, A. Kerambrun, J. C. Angelique, G. Auger, G. Bizard, R. Brou, C. Cabot, E. Crema, D. Cussol, D. Durand, Y. El Masri, P. Eudes, M. Gonin, K. Hagel, Z. Y. He, S. C. Jeong, C. Lebrun, J. P. Patry, A. Peghaire, J. Peter, R. Regimbart, E. Rosato, F. Saint-Laurent, B. Tamain, E. Vient, and R. Wada, Phys. Rev. Lett. **76**, 4895 (1996).

[5] G. Casini, A. A. Stefanini, M. Bini, P. R. Maurenzig, A. Olmi, G. Poggi, R. J. Charity, R. Freifelder, A. Gobbi, K. D. Hildenbrand, M. H. Tanaka, and J. P. Wessels, Phys. Rev. Lett. **67**, 3364 (1991).

[6] R. J. Charity *et al.*, Z. Phys. A **341**, 53 (1991).

[7] D. Jouan *et al.*, Z. Phys. A **340**, 63 (1991).

[8] L. Gingras, A. Chernomoretz, Y. Larochelle, Z. Y. He, L. Beaulieu, G. C. Ball, F. Grenier, D. Horn, R. Roy, M. Samri, C. St-Pierre, D. Thériault, and S. Turbide, Phys. Rev. C **65**, 061604(R) (2002).

[9] D. Dore, C. Volant, J. Cugnon, R. Legrain, G. Auger, C. O. Bacri, N. Bellaize, B. Borderie, R. Bougault, B. Bouriquet, R. Brou, P. Buchet, J. L. Charvet, A. Chbihi, J. Colin, D. Cussol, R. Dayras, A. Demeyer, D. Durand, J. D. Frankland, E. Galichet, E. Genouin-Duhamel, E. Gerlic, D. Guinet, B. Guiot, S. Hudan, P. Lautesse, F. Lavaud, J. L. Laville, J. F. Lecolley, C. Leduc, N. Le Neindre, O. Lopez, M. Louvel, A. M. Maskay, L. Nalpas, J. Normand, P. Pawlowski, M. Parlog, E. Plagnol, M. F. Rivet, E. Rosato, F. Saint-Laurent, J. C. Steckmeyer, G. Tabacaru, B. Tamain, L. Tassan-Got, E. Vient, and J. P. Wieleczko, Phys. Rev. C **63**, 034612 (2001).

[10] J. Péter *et al.*, Phys. Lett. B **237**, 187 (1990).

[11] M. Di Toro, A. Olmi, and R. Roy, Eur. Phys. J. A **30**, 65 (2006).

[12] L. Stuttgé *et al.*, Nucl. Phys. A **539**, 511 (1992).

[13] G. Casini, P. G. Bizzeti, P. R. Maurenzig, A. Olmi, A. A. Stefanini, J. P. Wessels, R. J. Charity, R. Freifelder, A. Gobbi, N. Herrmann, K. D. Hildenbrand, and H. Stelzer, Phys. Rev. Lett. **71**, 2567 (1993).

[14] C. P. Montoya, W. G. Lynch, D. R. Bowman, G. F. Peaslee, N. Carlin, R. T. de Souza, C. K. Gelbke, W. G. Gong, Y. D. Kim, M. A. Lisa, L. Phair, M. B. Tsang, J. B. Webster, C. Williams, N. Colonna, K. Hanold, M. A. McMahan, G. J. Wozniak, and L. G. Moretto, Phys. Rev. Lett. **73**, 3070 (1994).

[15] J. F. Lecolley *et al.*, Phys. Lett. B **354**, 202 (1995).

[16] P. Eudes, Z. Basrak, F. Sébille, V. de la Mota, and G. Royer, Phys. Rev. C **90**, 034609 (2014).

[17] S. C. Jeong *et al.*, Nucl. Phys. A **604**, 208 (1996).

[18] N. Marie *et al.*, Phys. Lett. B **391**, 15 (1997).

[19] L. Beaulieu, Y. Larochelle, L. Gingras, G. C. Ball, D. R. Bowman, B. Djerroud, D. Doré, A. Galindo-Uribarri, D. Guinet, E. Hagberg, D. Horn, R. Laforest, P. Lautesse, R. Roy, M. Samri, and C. St-Pierre, Phys. Rev. Lett. **77**, 462 (1996).

[20] V. Viola and R. Bougault, Eur. Phys. J. A **30**, 215 (2006).

[21] J. Pouthas *et al.*, Nucl. Instrum. Methods Phys. Res., Sect. A **357**, 418 (1995).

[22] D. Durand, Nucl. Phys. A **541**, 266 (1992).

[23] J. C. Steckmeyer *et al.*, Nucl. Phys. A **686**, 537 (2001).

[24] E. Vient *et al.*, Nucl. Phys. A **700**, 555 (2002).

[25] J. Łukasik *et al.*, Phys. Rev. C **55**, 1906 (1997).

[26] D. Lacroix, A. Van Lauwe, and D. Durand, Phys. Rev. C **69**, 054604 (2004).

[27] E. Vient, Habilitation à diriger des recherches, Université de Caen, 2006, https://tel.archives-ouvertes.fr/tel-00141924

[28] P. Eudes, Z. Basrak, and F. Sébille, Phys. Rev. C **56**, 2003 (1997).

[29] J. Colin, D. Cussol, J. Normand, N. Bellaize, R. Bougault, A. M. Buta, D. Durand, O. Lopez, L. Manduci, J. Marie, J. C. Steckmeyer, B. Tamain, A. VanLauwe, E. Vient, B. Borderie, F. Lavaud, N. LeNiendre, P. Pawlowski, E. Plagnol, M. F. Rivet, B. Bouriquet, A. Chbihi, J. D. Frankland, B. Guiot, S. Hudan, J. P. Wieleczko, J. L. Charvet, R. Dayras, L. Nalpas, C. Volant, E. Galichet, D. Guinet, P. Lautesse, M. Parlog, E. Rosato, M. Vigilante, and R. Roy, Phys. Rev. C **67**, 064603 (2003).

[30] J. Normand, Ph.D. thesis, Université de Caen, 2001 (unpublished).

[31] T. Lefort *et al.*, Nucl. Phys. A **662**, 397 (2000).

[32] M. Pichon *et al.*, Nucl. Phys. A **779**, 267 (2006).

[33] E. Bonnet, D. Mercier, B. Borderie, F. Gulminelli, M. F. Rivet, B. Tamain, R. Bougault, A. Chbihi, R. Dayras, J. D. Frankland, E. Galichet, F. Gagnon-Moisan, D. Guinet, P. Lautesse, J. Łukasik, N. LeNeindre, M. Parlog, E. Rosato, R. Roy, M. Vigilante, J. P. Wieleczko, and B. Zwieglinski, Phys. Rev. Lett. **103**, 072701 (2009).

[34] M. Bruno, F. Gulminelli, F. Cannata, M. D'Agostino, F. Gramegna, and G. Vannini, Nucl. Phys. A **807**, 48 (2008).

[35] E. Vient *et al.*, Nucl. Phys. A **571**, 588 (1994).

[36] Y.-G. Ma *et al.*, Phys. Lett. B **390**, 41 (1997).

[37] E. Vient *et al.*, Phys. Rev. C **98**, 044612 (2018).